# ZnO for application in photocatalysis: from thin films to nanostructures

Alessandro Di Mauro (alessandro.dimauro@ct.infn.it),[1*] Maria Elena Fragalà (me.fragala@unict.it),[2] Vittorio Privitera (vittorio.privitera@cnr.it),[1] and Giuliana Impellizzeri (giuliana.impellizzeri@ct.infn.it) [1]

[1] CNR-IMM, Via S. Sofia 64, 95123 Catania, Italy

[2] Dipartimento di Scienze Chimiche and INSTM UdR Catania, Università di Catania, Viale Andrea Doria 6, 95100 Catania, Italy.

* Address correspondence to: alessandro.dimauro@ct.infn.it

**Keywords:** ZnO, photocataysis, nanostructures, atomic layer deposition, electrospinning, nanorods.

## Abstract

In this research work, we report the photocatalytic properties of ZnO synthesized in several forms: ZnO thin films deposited by atomic layer deposition (ALD), ZnO nanofibers synthesized by electrospinnig, and ZnO nanorods realized by chemical bath deposition onto ZnO thin films grown by ALD. The methylene blue was employed as a representative dye pollutant to evaluate the photocatalytic activity of the samples. All the nanostructured materials showed an enhancement of the photocatalytic activity with respect to the thin films. It was found that ZnO nanorods deposited onto 3 nm thin film showed the best photocatalytic activity. The relevance of the results is discussed, opening the route for the application of ZnO in photocatalysis.

## Introduction

One of the most abundant clean energy source available in the world is the solar energy. Lewis in 2007 estimated that the solar energy striking our Earth in an hour is higher than the energy consumed by humans for an entire year [1]. For this reason, recently, the researcher's studies are focused on the development of materials that can efficiently harvest solar irradiation and use it for green environmental pollution management. In this field, photocatalysis is an interesting solution because it can use the renewable solar energy to activate the oxidation and reduction processes responsible for the removal of persistent and toxic organic compounds, and microorganisms in water [2]. During a typical photocatalytic process two different reactions occurs at the surface of the materials in contact with the wastewater: 1) an oxidation reaction, thanks to the photo-induced positive holes, 2) a reduction reaction, thanks to the photo-induced negative electrons [3]. Several kinds of semiconductor-based photocatalysts, such as titanium dioxide ($TiO_2$), zinc oxide (ZnO), iron(III) oxide ($Fe_2O_3$), zirconia ($ZrO_2$), tungsten trioxide ($WO_3$), and tantalum pentoxide ($Ta_2O_5$) have been applied in wastewater treatment [2,4-14].

In this field, ZnO has emerged as a promising candidate for environmental applications because it has a direct and wide band-gap energy in the near-UV spectral region, a strong oxidation ability, a great photocatalytic property, and a large free-exciton binding energy [15-19] so that exciton emission processes can persist at or even above the room temperature. The ZnO is easy to grow, and its thermodynamically stable phase is the hexagonal wurtzite structure [20-22]. In addition, the ZnO is an environmental friendly material as it is compatible with living organisms, which lending itself nicely to a broad range of daily applications that will not leave any risks to human health, and environmental impacts [21]. The ZnO has the same band-gap of $TiO_2$ (~ 3 eV) and for this reason it is expected a similar photocatalytic efficiency of $TiO_2$. Moreover, ZnO is relatively cheaper compared to $TiO_2$, whereby the usage of $TiO_2$ are uneconomic for large scale water treatment operations [23].

In order to improve the photocatalytic performance of semiconductor materials, different strategies can be employed, such as the nanostructuration, that offers a high surface-area–to-volume ratio, enhancing in this way the amount of the photo-generated charge carriers [6, 24-26]; or the use of metal nanoparticles in order to increase the electron-hole separation [5,27].

In this work we presented the photocatalytic activity of ZnO. Several kinds of ZnO were investigated: thin films deposited by atomic layer deposition (ALD), ZnO nanofibers (hereafter simply called "ZnO NFs") synthesized by electrospinning, and ZnO nanorods (hereafter simply called "ZnO NRs") synthesized by chemical bath deposition (CBD) on ZnO thin films grown by ALD. The idea was to follow the effect of the nanostructuration of the material on its photocatalytic response. Figure 1 reports a schematic of the materials presented in this review.

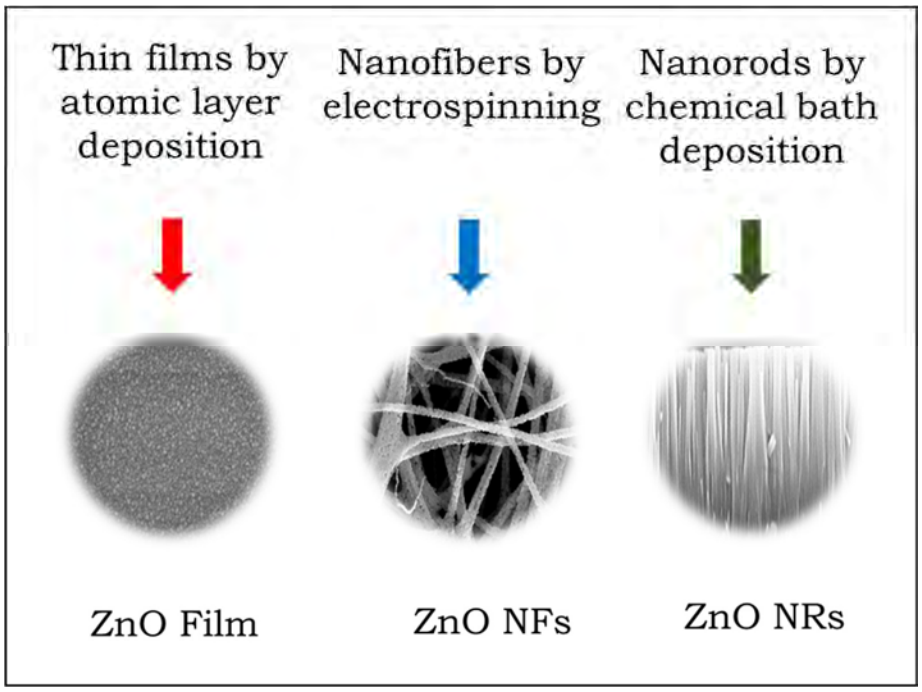


**Fig. 1** Schematic of ZnO nanomaterials presented in the review: thin films deposited by atomic layer deposition, nanofibers (ZnO NFs) deposited by electrospinning, and nanorods (ZnO NRs) realized by chemical bath deposition.

## Experimental

ZnO films with different thicknesses (from ~ 3 to ~ 30 nm) were deposited by ALD using the Picosun R-200 Advanced reactor. During the deposition the temperature was fixed at 300 °C, or 80 °C in the case of deposition on thermally-fragile plastic. Diethyl zinc (DEZ, purity 99.9999%) and de-ionized water were used as precursors, while $N_2$ was used as carrier and purge gas (purity ≥ 99.999%). The pulse and purge time were kept constant at 0.1/3/0.1/5 s for DEZ/$N_2$/$H_2O$/$N_2$. Three different substrates were used: silicon for the morphological and structural analyses, and for the photocatalytic tests; quartz for the optical measurements; poly methyl methacrylate (PMMA) in order to transfer the process on a flexible support. The PMMA film used as substrate was prepared according to the method of sonication and solution casting [28]. In detail, 800 mg of PMMA powders (molecular weight: 120000 a.m.u., transition temperature: 105 °C, density: 1.188 g/mL, as provided by Sigma-Aldrich) were dissolved in 4 ml of acetone. After that, the mixture was cast into a Petri dish (6 cm in diameter) and dried overnight to produce a PMMA film that was peeled off from the Petri dish.

The thickness of the ZnO films deposited on silicon substrates by ALD was evaluated by the M-2000 spectroscopic ellipsometer by Woollam, by applying a Cauchy model.

The synthesis of ZnO NFs was achieved by electrospinning. A solution containing 1 g of polyvinylpyrrolidone (PVP) polymer (molecular weight: 1300000 a.m.u.), and 0.36 g of zinc acetate ($Zn(CH_3COO)_2 \cdot H_2O$) in 2 ml of dimethylformamide (DMF) (all reagents were purchased from Sigma Aldrich), was electrospun using the electrospinning equipment EC-DIG Electrospinning by the IME Technologies. The composite was ejected from the needle (21 gauge) of a syringe applying an electrical field as high as several kV/cm; in detail, the depositions were achieved by using a negative and positive voltage of -4 and 18 kV, respectively. Nanofibers were collected (in a stationary mode) on the surface of silicon substrates clamped on top of a conductive circular collector. In order to remove

the PVP matrix, the ZnO nanofibers were annealed at 500 °C for 1 hr, in a conventional horizontal furnace under a controlled oxygen atmosphere ($O_2$ flow: 2.5 l/min) [29].

Well-aligned ZnO NRs arrays were synthesized using the CBD method. ZnO thin films deposited by ALD were used as seeds for the CBD. The seed layers were dipped horizontally (with the face down) in a 0.025 M zinc acetate dehydrate and 0.025 M ethylenediamine aqueous solutions under mild stirring at 80 °C for 3 hrs [30-31]. The obtained ZnO NRs were washed with de-ionized water and sonicated for 3 min, so to clean the surface, and then dried by blowing $N_2$.

A schematic of the ZnO materials is reported in Fig. 1.

All the synthesized materials were observed by the Zeiss Supra-55 field emission scanning electron microscope (SEM), operating at 5.0 keV, equipped with an Oxford solid state detector for energy dispersed X-ray spectroscopy (EDS).

The crystallographic structure of the materials was analysed by X-ray diffraction (XRD) with a Brucker D-500 diffractometer (detector scan mode) at 0.8° angle of incidence, and 2θ from 20° to 60°. The XRD spectra were analysed by the Bruker software suite, including ICSD structure database.

The optical characterization was obtained by extracting both the normal transmittance (T) and the 8° reflectance (R) spectra in the 200–800 nm wavelength range, by using a Perkin-Elmer Lambda 40 UV/VIS/NIR spectrophotometer.

The photocatalytic activity of the investigated materials was tested by the degradation of methylene blue (MB) dye. Before starting the MB degradation experiments, the samples were irradiated by an UV lamp for 60 min in order to remove the hydrocarbons from the sample surfaces [32]. ZnO thin films, ZnO NFs and ZnO NRs arrays deposited on Si substrates (1 $cm^2$ in size) were immersed in 2 ml of dye aqueous solutions ($1.5 \times 10^{-5}$ M). The pH of the aqueous solution is one of the most important operating parameter that affects the heterogeneous photocatalysis, since it influences the surface-charge properties of the photocatalyst, and the position of the conductance and valence

bands. Some papers reports the effects of the pH on the photocatalytic activity of ZnO (the reader can refer to Refs. [33-35]). It is shown that the ZnO photocatalytic rate increases with the pH, reaching high rate for 7.5 pH. For this reason, the measurements were performed at a fixed pH value of 7.5, using NaOH to control its value. The dye solution containing the samples was irradiated by an UV lamp with the irradiance of 2 $mW/cm^2$, which simulate the UV irradiance of the Sun on the Earth. The irradiated solution was measured at regular time intervals with the Lambda 45 Perkin-Elmer UV/VIS/NIR spectrophotometer, in a wavelength range of 500-800 nm. The degradation of MB was quantitatively evaluated by the absorbance peak at 664 nm in the Lambert-Beer regime [36]. The photo-degradation reaction rate was calculated from the linear plot of $-\ln(C_0/C)$ versus the irradiation time (where $C_0$ is the starting concentration of the MB, $C$ is the concentration of the MB at the time $t$) [37]. The decomposition of the MB dye in the absence of any photocatalyst materials was always checked as a reference. Control experiments in the dark for 60 min were conducted in order to clarify the contribution of the adsorption of the MB at the beaker walls and at the sample surface.

**Results**

Several films of ZnO were deposited by ALD at 300 °C with different thickness: 3, 5, 10, 20, and 30 nm, by simply varying the number of the ALD cycles. The surface morphology of the 3, 10, and 30 nm thick films was reported in Fig. 2.

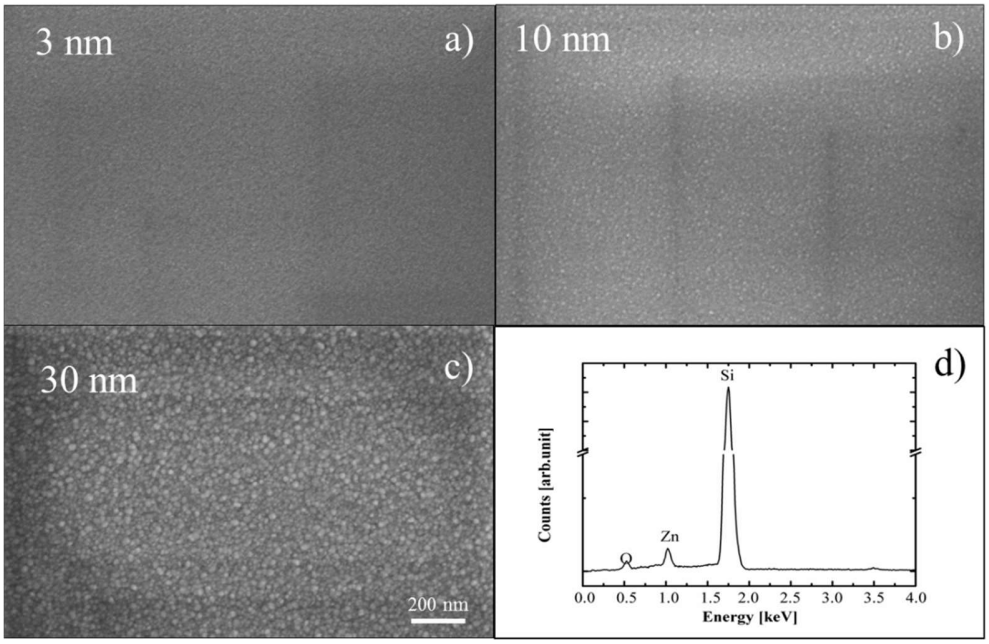


**Fig. 2** Plan-view SEM analyses of ZnO thin films: 3 nm (a), 10 nm (b), and 30 nm (c) thick, deposited at 300 °C. Figure (d) reports the EDS analysis of the 30 nm thick sample.

The plan-view SEM images showed a high uniformity of the ALD films, with a granularity that increases with the thickness (see Fig. 2 (a), (b), and (c)), in good agreement with what reported in literature for atomic layer deposition of ZnO [38]. The EDS analysis of the 30 nm thick sample (Fig. 2 (d)) shows the typical peak of the Zn (at ~ 1.0 keV), O (at ~ 0.5 keV) both coming from the ZnO, and the peak of the Si (at ~ 1.7 keV) due to the silicon substrate. The films with lower thickness showed similar spectra, for this reason they are not reported.

The XRD spectra of the ZnO films are reported in our previous article [39], showing the typical pattern of the wurtzite structure.

The ZnO films were also analyzed by optical characterization, so to evaluate the band-gap energy of the films. In Fig. 3 the absorbance ($A$) of the films as a function of the wavelength is reported. The

absorbance was calculated by the transmittance ($T$) and the reflectance ($R$) spectra through to the following equation:

$$A\% = 100\% - T\% - R\% \quad (1)$$

All the films showed the typical optical absorption in the UV part of the spectrum. Moreover, the intensity of the absorbance increases with the film thickness, as expected. The optical spectra were analyzed by the Tauc model in order to evaluate the band-gap energy of the ZnO films. The model was born for the description of the light absorption process in amorphous semiconductors [40], but the applicability of the model for polycrystalline semiconductors was demonstrated. In detail, Viezbicke *et al.* [41] showed that the optical absorption strength depends on the difference between the photon energy and the band-gap energy as follows:

$$(\alpha h\nu)^{1/n} = B(h\nu - E_g) \quad (2)$$

where $\alpha$ is the absorption coefficient, $h$ is the Plank's constant, $v$ is the photon's frequency, $B$ is a proportionality constant, $E_g$ is the optical band-gap of the material. The value of the exponent denotes the nature of the electronic transition, and $n$ is ½ for direct allowed transitions, which is the case of ZnO [42]. The absorption coefficient were extracted from the transmittance ($T$) and reflectance ($R$) spectra by using the following equation [43]:

$$\alpha = \frac{1}{d} ln \frac{T_Q(1 - R_S)}{T_S} \quad (3)$$

where $d$ is the thickness of the film; the subscripts $Q$ and $S$ refer to the quartz and the sample, respectively. The inset of Fig. 3 reports the plot $(\alpha h\nu)^2$ versus $h\nu$ (i.e., the Tauc plot), that allowed the direct determination of the $E_g$. The optical band-gap for the ZnO films resulted 3.3, 3.2, and 3.2 eV for the samples with a thickness of 3, 10, and 30 nm, respectively. Assuming an error of ~ 10% in the

estimation of the optical band-gap, we can conclude that the band-gap is the same for the different thicknesses, and it is in perfect agreement with the value of 3.3 eV reported in literature [42].

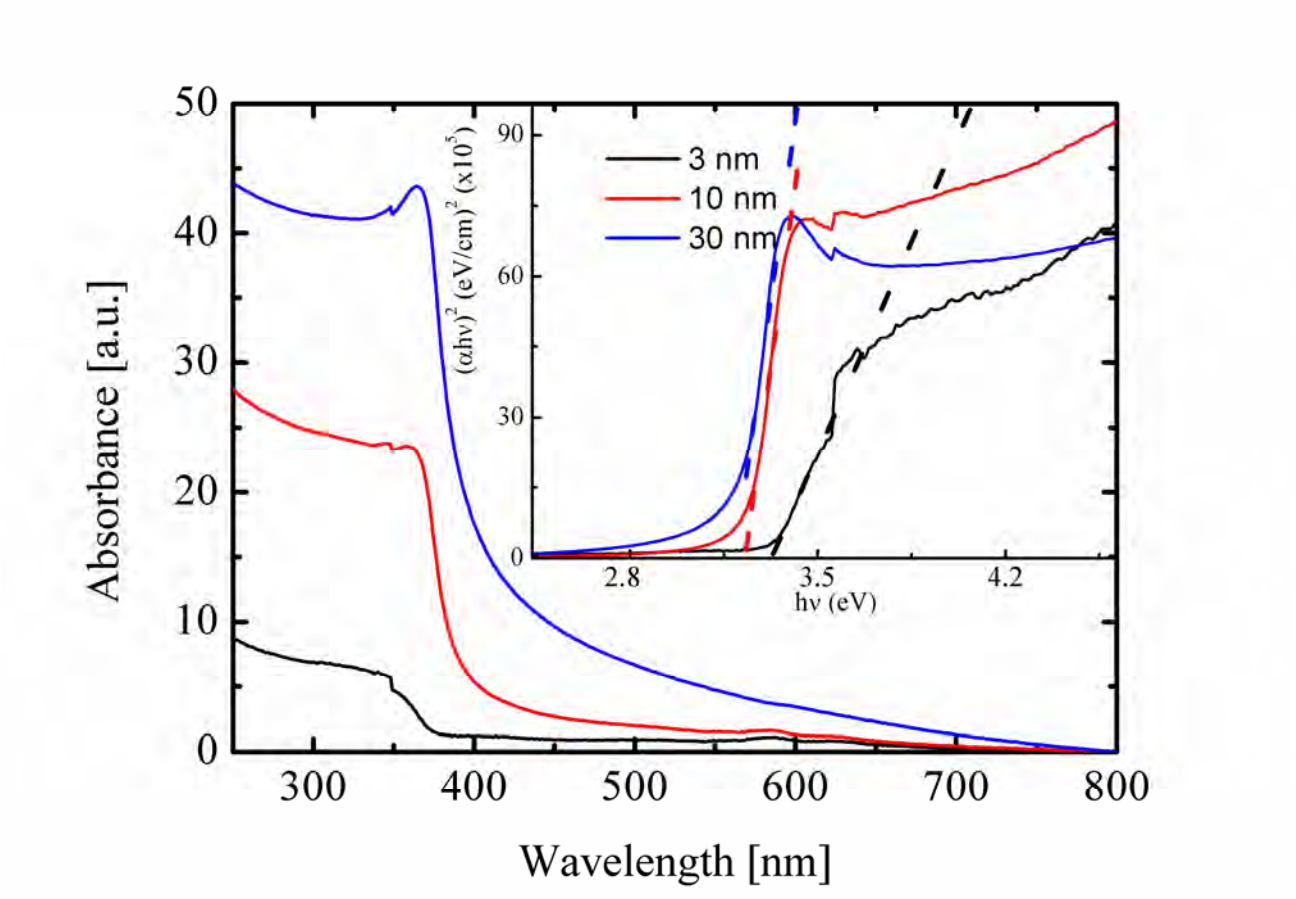


**Fig. 3** Absorbance spectra of 3, 10, 30 nm thick ZnO films. The Tauc plots are reported in the inset.

The photo-degradation of the MB dye under UV light irradiation was investigated in order to understand the correlation between the thickness and the photocatalytic activity of the films. First of all, the samples were dipped in a MB aqueous solution and held in dark conditions for 60 min, for the evaluation of the degree of the adsorption of MB on the beaker walls and on the sample surface. The adsorption is reported in grey colour in Fig. 4 (a). The figure shows the evolution of the concentration of MB versus the time, where $C$ is the concentration of MB at time $t$, and $C_0$ is the starting

concentration of MB. Since the adsorption value is only ~ 1%, that is equal to the experimental error of the discoloration measurements, we can affirm that the ZnO films do not adsorb the MB.

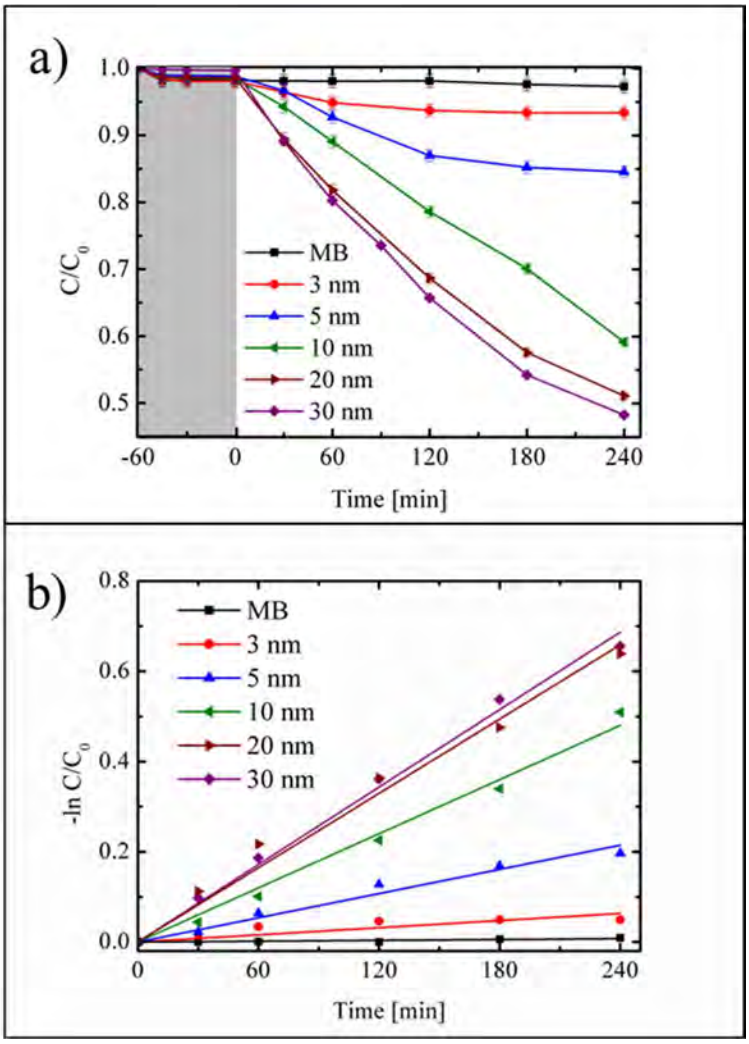


**Fig. 4** (a) MB photo-degradation under UV irradiation for six samples: MB (squares), MB with the ZnO thin films: 3 nm thick (circles), 5 nm thick (up triangles), 10 nm thick (left triangles), 20 nm thick (right triangles), and 30 nm thick (diamonds). (b) $-\ln(C/C_0)$ versus the irradiation time for ZnO thin films.

Thereafter, we evaluated the photo-degradation of ZnO deposited at 300 °C for all the five thicknesses, comparing the degradation to the one of a solution without any catalysts (squares in Fig. 4 (a)). The photocatalytic activity clearly increases with the thickness, because more charge carries are generated

by photo-absorption. On the other hand, the photocatalytic activity starts to saturate for a film thickness of ~ 20 nm. This means that the charge carriers, generated by the irradiation, are not able to diffuse for more that 20 nm so to reach the interface of the film in contact with the polluted water, since they recombine before reaching the surface, and as a consequence they do not contribute to the photoreactions.

In order to quantify the photocatalytic activity of the films, we used the formula of a pseudo first order process studied by Langmuir and Hishelwood:

$$ln\frac{C}{C_0} = -kt \quad (4)$$

where $k$ is the photo-degradation rate and $t$ is the irradiation time [34] (see Fig. 4 (b)). In Table 1 we reported the values of the photo-degradation rate, for the different film thicknesses.

| **Thickness (nm)** | **k ($min^{-1}$)** |
|---|---|
| 0 | $(6.3 \pm 0.3) \times 10^{-5}$ |
| 3 | $(6.0 \pm 0.3) \times 10^{-4}$ |
| 5 | $(9.0 \pm 0.5) \times 10^{-4}$ |
| 10 | $(2.1 \pm 0.1) \times 10^{-3}$ |
| 20 | $(2.8 \pm 0.1) \times 10^{-3} \pm 1x10^{-4}$ |
| 30 | $(2.8 \pm 0.1) \times 10^{-3}$ |

Tab.1 Photo-degradation rate for the different film thicknesses

The values of the photo-degradation rate resulted higher than the ones reported in literature for $TiO_2$ thin film, grown in the same conditions [44]. In a previous work, we evaluated the diffusion

length of the charge carriers in ZnO thin films deposited by ALD at 80 °C [39]. Here we reported the evaluation of the diffusion length of the charge carriers for samples grown at 300 °C (Fig. 5).

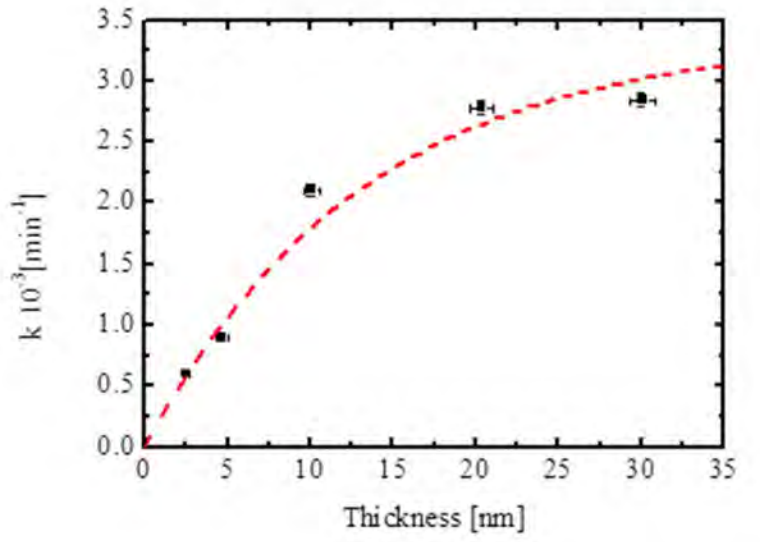


**Fig. 5** Reaction rate, *k*, plotted as a function of the film thickness (squares). The best fit of the experimental data is reported with dashed line.

The charge diffusion length, normal to the surface, was obtained by fitting the increase of the photocatalytic activity with the increase of the film thickness by the following exponential law [39]:

$$k = D\left(1 - e^{-\frac{d}{\lambda}}\right) \quad (5)$$

where $k$ is the measured photo-degradation rate, $d$ is the film thickness, $D$ and $\lambda$ are two fitting parameters, in particular $D$ correspond to the photocatalytic activity of very thick films, while $\lambda$ indicates the distance from the surface at which a charge carrier has a probability 1/e to reach the surface. The best fit of the experimental data gives a value for $\lambda$ of (13.3 ± 0.8) nm, and $D$ (3.2 ± 0.2) × $10^{-3}$ $min^{-1}$. The $\lambda$ value resulted slightly higher than the value found for the films grown at 80 °C: (10.7

± 0.7) nm [45]; probably this is the consequence of a lower amount of defects due to the higher deposition temperature, that clearly favors the diffusion length of the charge carriers.

The high performance of the ZnO thin films in terms of photo-degradation drove us to fabricate a flexible materials by depositing ZnO by ALD on a plastic film. In particular, once the film thickness (~ 20 nm) was optimized, we transferred the ALD process on PMMA. The PMMA was chosen for its transparency to visible light, mechanical properties, chemical stability, low-cost and suitability to stay in contact with food and drinks. In Fig. 6 we reported the morphology of the ZnO films, deposited at 80 °C, with a thickness of 20 nm, on Si substrate (a), or on PMMA (b).

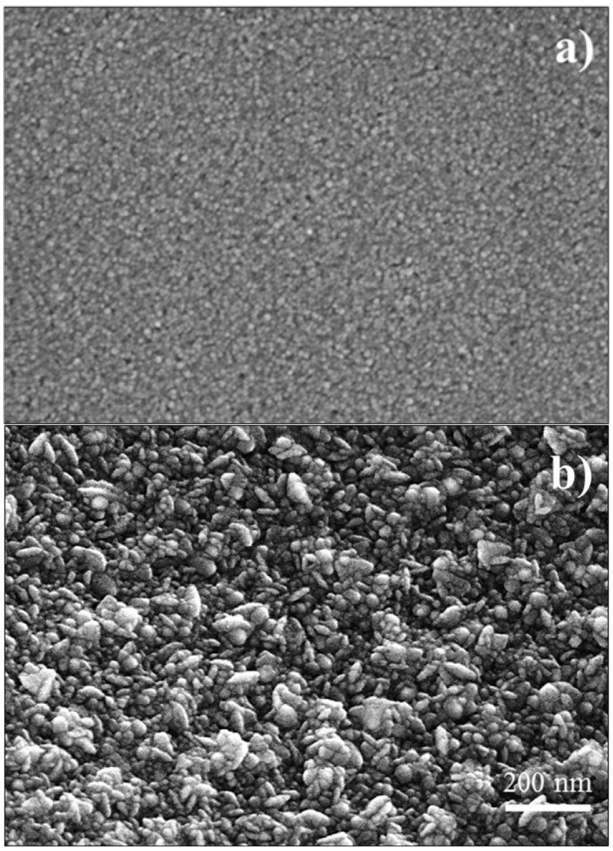


**Fig. 6** Plan-view SEM analyses of ZnO films, 20 nm thick, deposited at 80 °C on Si (a), or on PMMA (b).

The films deposited on PMMA showed a higher roughness than the film grown on Si, as expected. Indeed the surface of the bare polymer is more irregular than the silicon surface, causing as a consequence the different observed morphology.

The crystallinity of both samples was investigated in order to exclude a possible effect of the substrates on the grown films. It is worth to note that the crystallinity is an important property for the photocatalytic efficiency of a material [39] because it strongly influence the recombination probability of the charge carriers. The XRD patterns of the two ZnO films deposited on Si substrate or on PMMA are reported in Fig. 7.

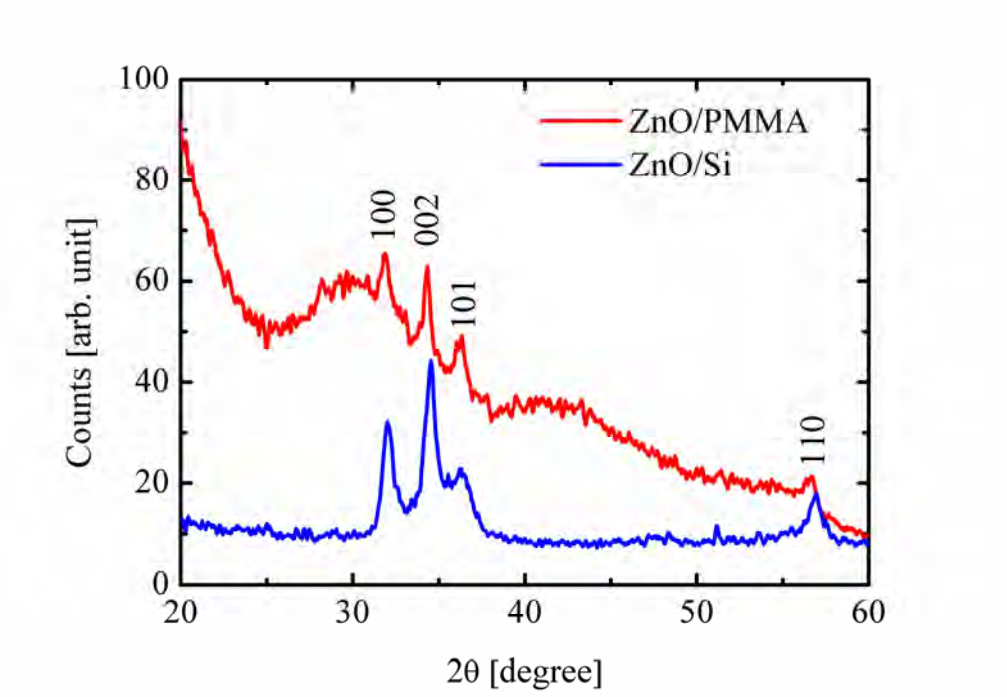


**Fig. 7** XRD patterns of ZnO films, 20 nm thick, deposited at 80 °C on Si (down), or on PMMA (up).

Both samples were polycrystalline with the wurtzite structure, indeed the typical peaks of the wurtzite: (100), (002), (101), and (110) are clearly visible. The XRD pattern of the ZnO sample grown on the PMMA substrate showed in addition two broad bands related to the amorphous structure of the

polymer. The crystallinity of the ZnO film deposited on PMMA is hence an evidence that the growth of the ZnO film is not influenced by the substrate used for the deposition.

Figure 8 shows the photocatalytic activity of the ZnO films deposited at 80 °C on Si substrate (down triangles) and on PMMA (circles) under UV light irradiation. An aqueous dye solution, only containing the MB, was used as reference (squares in Fig. 8).

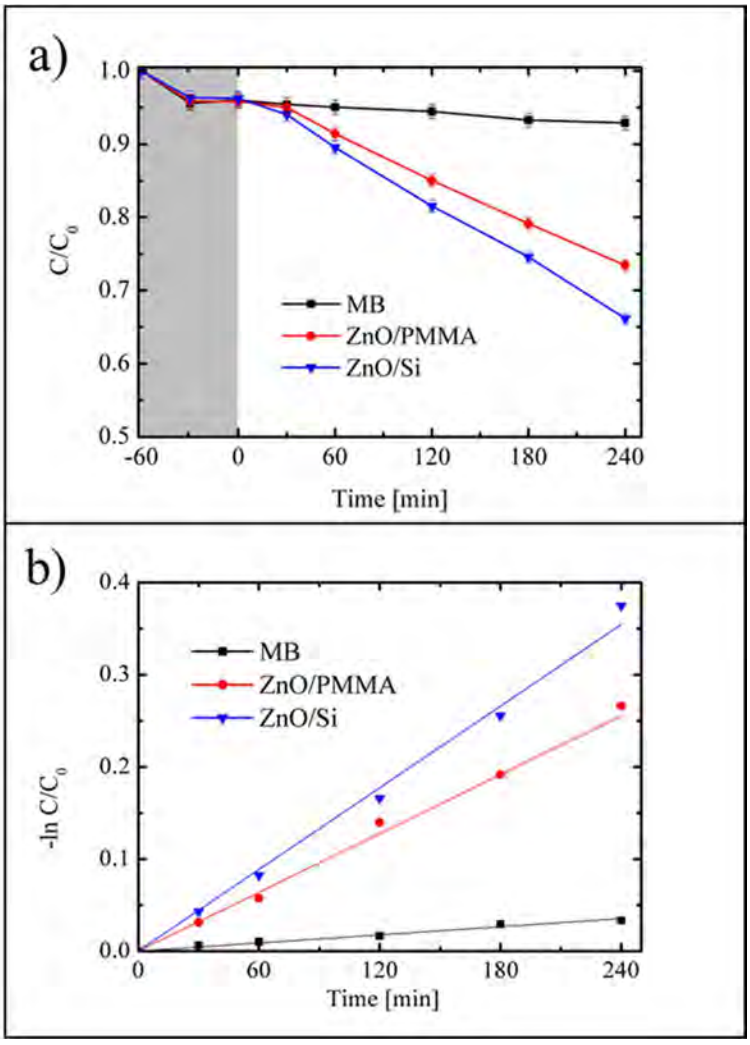


**Fig. 8** (a) MB photo-degradation under UV irradiation for three samples: MB (squares), MB with the ZnO film deposited on PMMA (circles), or on Si substrate (down triangles). (b) $-\ln(C/C_0)$ versus the irradiation time for ZnO films on PMMA substrate (circles), or on Si (down triangles).

The MB solution did not show any degradation, as expected, instead the films of ZnO showed a significant photocatalytic activity. We calculated the values of the kinetic constants (see Fig. 8 (b)) for the two ZnO films, obtaining the following results: $(1.1 \pm 0.1) \times 10^{-3}$ and $(1.5 \pm 0.1) \times 10^{-3}$ $min^{-1}$ for the ZnO films deposited on PMMA and on Si substrate, respectively. In Fig. 9 we reported the ratio between the kinetic constants of the photo-degradation process for the ZnO films grown on Si or on PMMA and the kinetic constant for the MB solution. In the abscissa axis, 'MB' indicates the MB decomposition in the absence of any sample, that is 1 due to the normalization done (i.e., $k/k_{MB}$); "ZnO/PMMA" and "ZnO/Si" refer to the MB solution in which we put the ZnO film grown on PMMA or on Si, respectively. The photo-degradation reaction rate with respect to the MB kinetic constant resulted 35% and 40% for ZnO on PMMA or on Si, respectively.

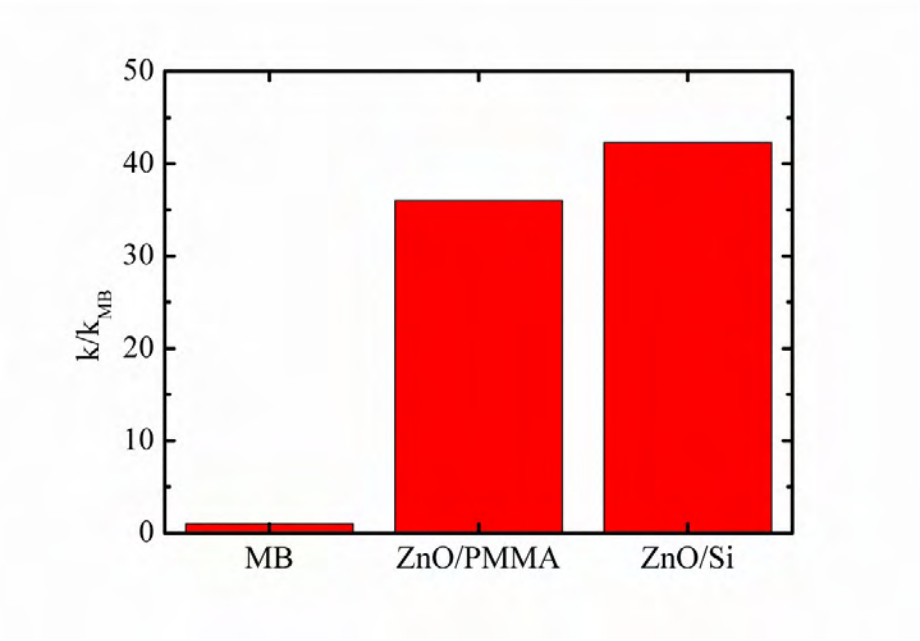


**Fig.9** Photo-degradation reaction rate normalized to the value obtained for the MB in the absence of any catalyst for the different investigated samples: ZnO film on PMMA (ZnO/PMMA), ZnO film on Si (ZnO/Si).

As a consequence of the reported results, we can affirm it is possible and easy to synthesize ZnO thin films on a flexible substrate with a comparable photocatalytic activity to the ZnO film deposited on Si substrate.

In order to improve the interaction between the photocatalytic materials and the pollutants, a possible way is to increase the surface-area–to-volume ratio by the nanostructuration of the ZnO. Thus, we synthesized and tested two different nanostructures: ZnO nanofibers, and ZnO nanorods.

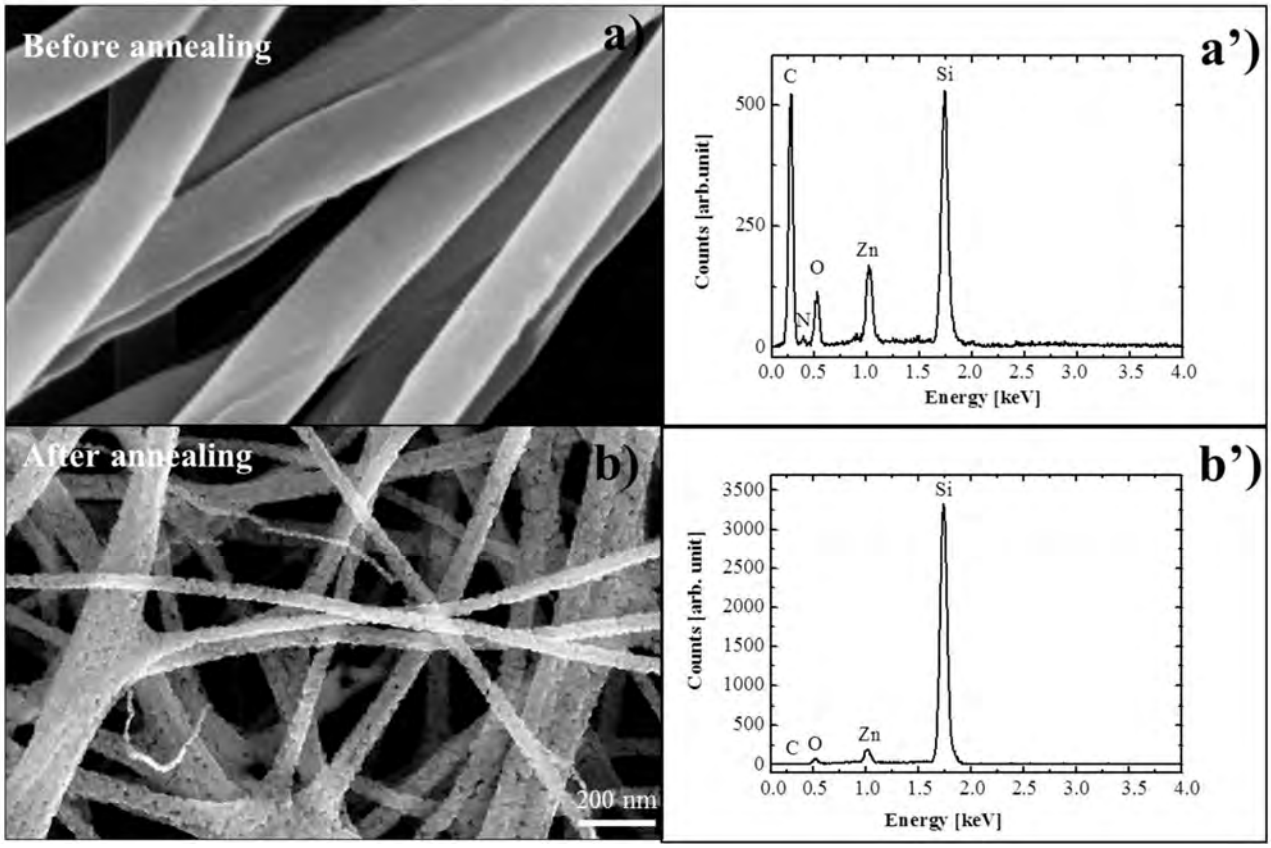


**Fig. 10** Plan-view SEM images of ZnO NFs before (a), and after the calcination (b), together with the EDS analyses (a'-b').

Figure 10 shows the morphology of ZnO NFs before (a), and after (b) the calcination process at 500 °C. The synthetized nanofibers show a random orientation, due to the instability of the electrospinning jet [45,46]. The mean fiber diameter, evaluated by Digital Micrograph 3.6.1 (Gatan Inc.), before the calcination process was ~ 160 nm, while after the calcination (the PVP matrix used for the electrospinning process was removed) the mean diameter resulted ~ 100 nm. The EDS analysis confirmed the complete combustion of the polymer; indeed, the spectrum of the ZnO NFs before the calcination process (Fig. 10 (a')) shows the peak of the C (at ~ 0.28 keV) and N (at ~ 0.40 keV), related to the presence of the PVP. After the calcinations, the C and N peaks disappeared and the intensity of the oxygen peak decreased, clearly demonstrating the removal of the polymeric matrix.

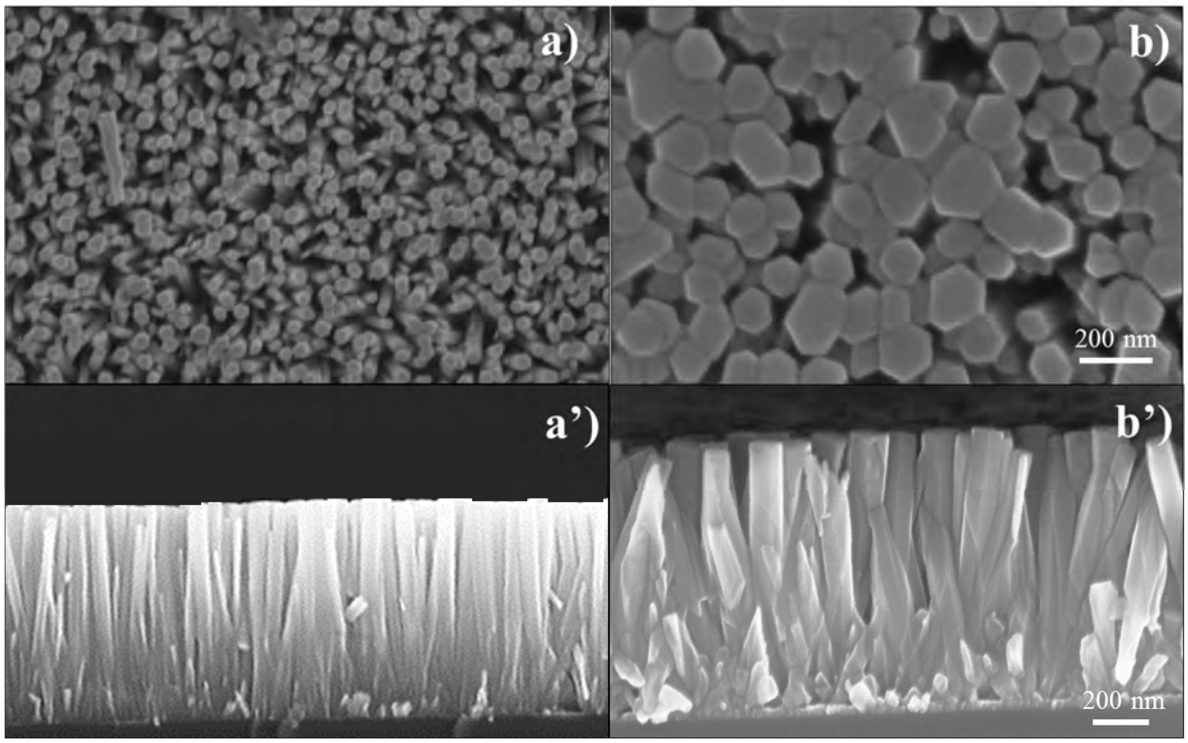


**Fig. 11** SEM images of ZnO NRs: (a) plan-view, and (a') cross-view of ZnO NRs grown on 3 nm thick seed layer; (b) plan-view, and (b') cross-view of ZnO NRs grown on 30 nm thick seed layer.

ZnO NRs were grown by CBD on ALD layers [47], used as seed in order to promote the growth. The SEM images pointed out the role of the seed layer thickness in modulating the ZnO NRs lateral dimension and length (Fig. 11). In detail, the SEM analyses in plan-view showed an increase of the lateral size of the NRs with the ALD film thickness. This increase was quantified by measuring the nanorod radii in several micrographs, by Digital Micrograph 3.6.1 (Gatan Ic.), and resulted ~ 28 nm for the 3 nm thick seed layer, ~ 74 nm for the 30 nm thick seed layer. The density of the ZnO NRs resulted higher for the 3 nm seed layer (117 NRs/$\mu m^2$), with respect to the 30 nm seed layer (23 NRs/$\mu m^2$). The cross-view SEM images clearly indicated a growth of well-aligned ZnO NRs. In detail, the NRs are found to growth along the (001) direction. This may be because the ZnO has a dipole moment along this direction; this dipole moment will try to align itself with charged ZnO thin film surface so to minimize energy [30]. The ZnO NRs height resulted ~ 700 nm for the 3 nm seed layer (see Fig. 11 (a')), while it resulted ~ 1100 nm for the 30 nm seed layer (see Fig. 11 (b')).

Figure 12 shows the photo-degradation of MB aqueous solution under UV light irradiation for the ZnO NFs and ZnO NRs.

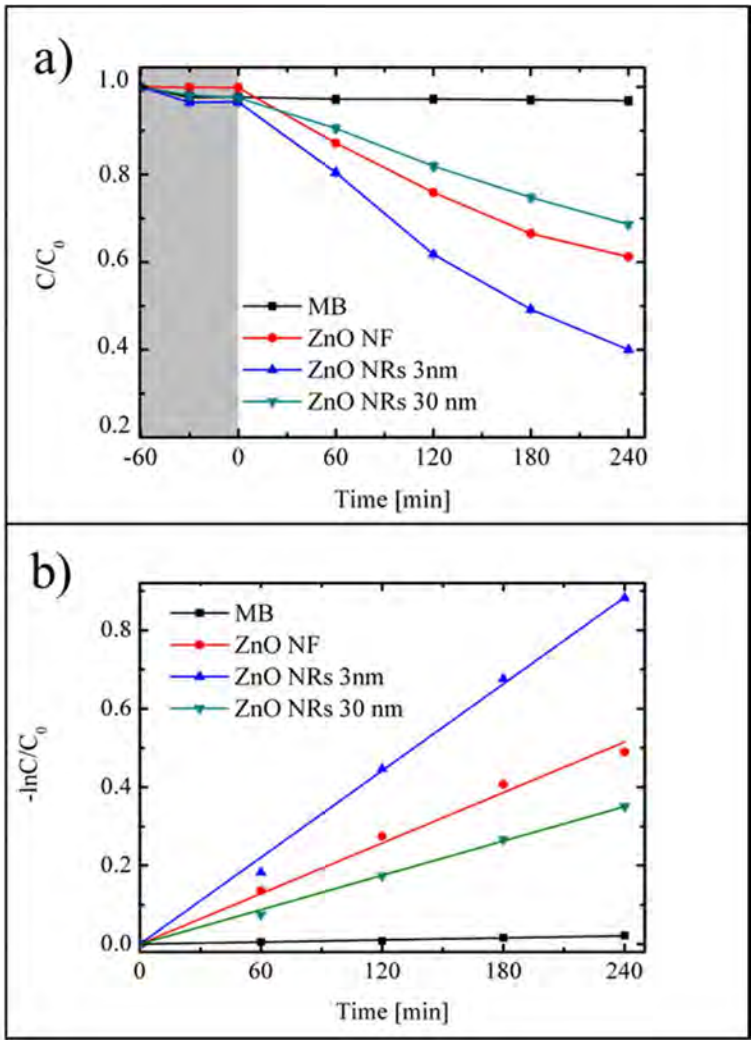


**Fig. 12** (a) MB photo-degradation under UV irradiation promoted by ZnO NFs (circles), ZnO NRs for the 3 nm seed layer (up triangles), and ZnO NRs for the 30 nm seed layer (down triangles). (b) $-\ln(C/C_0)$ versus the irradiation time for the same samples.

The photo-degradation reaction rate (see Fig 12 (b)): resulted $(2.7 \pm 0.1) \times 10^{-3}$, $2.3 \pm 0.1) \times 10^{-3}$, and $4.3 \pm 0.2) \times 10^{-3}$ $min^{-1}$ for the ZnO NFs, ZnO NRs for 30 nm seed layer, and ZnO NRs for 3 nm seed layer, respectively. The best photocatalytic performance was obtained for the ZnO NRs sample grown on 3 nm seed layer. This result can be understood considering that the photocatalytic reaction is a chemical reaction occurring at the material surface, as a consequence it is strongly affected by the exposed

surface area. In the present case we can assume that the enhancement in the exposed surface of the ZnO NRs grown on 3 nm seed layer is responsible for the improvement of the photocatalytic performance.

In order to summarize all the experimental results, we reported in Fig. 13 the photo-degradation reaction rate of MB, normalized to the value obtained for the MB decomposition in the absence of any photocatalyst. On the abscissa axis of Fig. 13, "MB" indicates the MB decomposition in the absence of any photocatalyst, that is always 1 due to the normalization done (i.e., $k/k_{MB}$); "Film 3 nm" and "Film 30 nm" refer to the MB decomposition in the presence of the ALD ZnO films (3 and 30 nm indicate the thickness of the films); "ZnO NFs" indicates the ZnO nanofibers; "NRs 3 nm" and "NRS 30 nm" refer to the ZnO NRs deposited on 3 nm and 30 nm seed layer, respectively. The nanostructuration of ZnO clearly caused an increase of the photo-degradation of MB dye compared to the thin films, due to an increase of the exposed surface area. The ZnO NRs deposited on 3 nm seed layer showed the highest photo-degradation reaction rate.

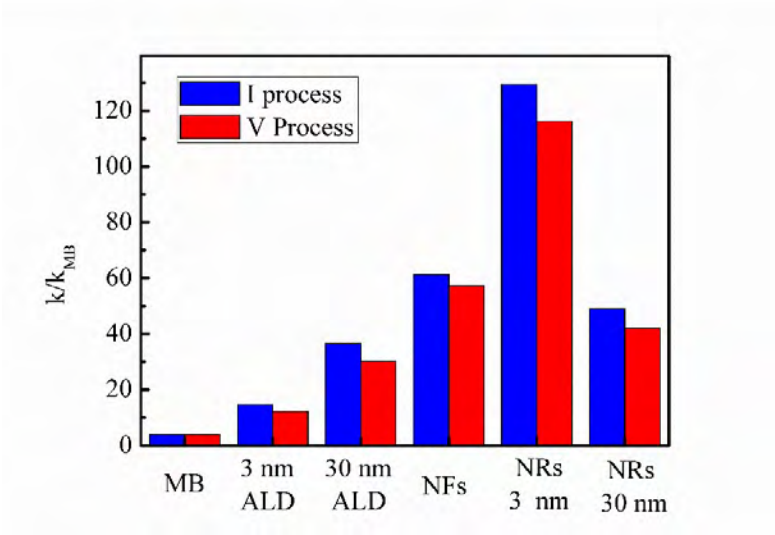


**Fig 13** Photo-degradation reaction rate, normalized to the value obtained for the MB in the absence of the catalyst, for the different investigated samples: ALD ZnO flat film ("3 nm ALD" and "30 nm ALD"), ZnO nanofibers ("NFs") and ZnO NRs grown onto 3 and 30 nm thin films ("3 nm NRs", and "30 nm NRs"), for the I (blue) and V process (red).

The photo-corrosion of ZnO during the photocatalytic process is a commonly observed phenomenon [48]. For this reason the stability of the synthetized nanomaterials was investigated, by repeating the photo-degradation measurements up to five times. In detail, at the end of each experiment the samples were immersed in de-ionized water under UV light irradiation for 2 hrs and then leaved in de-ionized water for 15 hrs, in order to remove any possible residues of the dye. The results for the V process were reported in Fig. 13. The measurements clearly show that after five processes the photo-degradation activity is reduced of only the 15%. These results demonstrate that the photo-corrosion phenomenon is negligible for the investigated samples.

**Conclusion:**

Here we reported an overview of the photocatalytic activity of different types of ZnO: ZnO thin films, ZnO nanofibers, and ZnO nanorods. In addition the deposition process of ZnO thin films by ALD was successfully transferred on polymer substrate (PMMA). Even if the ZnO thin films showed a significant photo-degradation of MB dye under UV light irradiation, the nanostructuration of the material strongly enhanced the photocatalytic performance. In particular, the electrospun ZnO nanofibers (~ 50 nm in mean radius) exhibited a photo-degradation reaction rate that is ~ 40 % higher than that observed for ZnO thin films. The best photocatalytic performance was obtained for ZnO NRs grown by CBD onto an extra-thin (3 nm) ALD seed layer, with an improvement of the photo-degradation reaction rate of ~ 100 % with respect to ZnO NFs. The reported results demonstrate that ZnO, both in the form of thin films, or in the form of nanofibers or nanorods, can be fruitfully employed for several photocatalytic applications, such us wastewater treatment.

**ACKNOWLEDGEMENT**

The authors wish to thank Giuseppe Pantè (CNR-IMM) for the technical assistance. This work has been supported by the FP7 European Project WATER (Grant Agreement 316082).

**References**

[1] N. S. Lewis, Science, 315 (2007) 798-801.

[2] X. Li, J. Yu, M. Jaroniec, Chem. Soc. Rev. 45 (2016) 2603–2636.

[3] A. Fujishima, X.T. Zhang, D.A. Tryk, Surf. Sci. Rep. 63 (2008) 515–582.

[4] R. Vinu, G. Madras, J. Indian Inst. Sci. 90 (2010) 189–229.

[5] V. Scuderi, G. Impellizzeri, L. Romano, M. Scuderi, M. V. Brundo, K. Bergum, M. Zimbone, R. Sanz, M. A. Buccheri, F. Simone, G. Nicotra, B. G. Svensson, M. G Grimaldi, V. Privitera, Nanoscale 6 (2014) 11189–11195.

[6] V. Scuderi, G. Impellizzeri, L. Romano, M. Scuderi, G. Nicotra, K. Bergum, A. Irrera, B. G. Svensson, V. Privitera, Nanoscale Res. Lett. 9 (2014) 458–465.

[7] G. Impellizzeri, V. Scuderi, L. Romano, E. Napolitani, R. Sanz, R. Carles, V.Privitera, J. Appl. Phys. 117 (2015) 105308.

[8] G. Impellizzeri, V. Scuderi, L. Romano, P. M. Sberna, E. Arcadipane, R. Sanz, M.Scuderi, G. Nicotra, M. Bayle, R. Carles, F. Simone, V. Privitera, J. Appl. Phys.116 (2014) 173507-1-8.

[9] M. M. Momeni, Z. Nazari, Ceram. Int. 42 (2016) 8691–8697.

[10] M. M. Momeni, M. Mirhosseini, M. Chavoshi, Ceram. Int. 42 (2016) 9133–9138.

[11] M. M. Momeni, Y. Ghayeb, M. Davarzad, J. Electroanal. Chem. 739 (2015) 149–155.

[12] K. M. Lee, A. H. Abdullah, Mater. Sci. Semicond. Process. 30 (2015) 298-306.

[13] A. Mirzaei, Z. Chen, F. Haghighat, L. Yerushalmi, Sustainable Cities and Society 27 (2016) 407-418.

[14] K. Mun Lee , C. Wei Lai, K. Sing Ngai, J. Ching Juan, Water Res. 88 (2016) 428-448.

[15] A. Janotti, C.G. Van de Walle, Rep. Prog. Phys. 72 (12) (2009) 126501.

[16] D. C. Reynolds, D. C. Look, B. Jogai, C. W. Litton, G. Cantwell, W. C. Harsch, Phys. Rev. B 60 (4) (1999) 2340–2344.

[17] Y. Chen, D. M. Bagnall, H.-J. Koh, K.-T. Park, K. Hiraga, Z.-Q. Zhu, T. Yao, J. Appl. Phys. 84 (7) (1998) 3912–3918.

[18] I. Udom, M. K. Ram, E. K. Stefanakos, A. F. Hepp, D. Y. Goswami, Mater. Sci. Semicond. Process. 16 (2013) 2070–2083.

[19] A. Kołodziejczak-Radzimska, T. Jesionowski, Materials, 7(4) (2014) 2833-2881.

[20] Z. Lin Wang, Mater. Today 7 (2004) 26-33.

[21] L. Schmidt-Mende, J. L. MacManus-Driscoll, Mater. Today 10 (5) (2007) 40-48.

[22] M. Tan Man, Ji-Hee Kim, M. S. Jeong, A. ThiDo, H. S. Lee, J. Lumin. 185 (2017) 17-22.

[23] N. Daneshvar, D. Salari, A.R.Khataee, J. Photochem. Photobiol. A: Chem. 162 (2-3) (2004) 317-322.

[24] M. M. Momeni, Appl. Surf. Sci. 357 (2015) 160–166.

[25] V. Scuderi, M. Zimbone, M. Miritello, G. Nicotra, G. Impellizzeri, V. Privitera, Beilstein J. Nanotechnol. 8 (2017) 190.

[26] V. Scuderi, G. Impellizzeri, M. Zimbone, R. Sanz, A. Di Mauro, M. A. Buccheri, M. P. Miritello, A. Terrasi, G. Rappazzo, G. Nicotra, V. Privitera, Appl. Catal. B: Environ. 183 (2016) 328.

[27] M. M. Momeni, Y. Ghaye, Appl. Phys. A 122 (2016) 620.

[28] M. Cantarella, R. Sanz, M. A. Buccheria, F. Ruffino, G. Rappazzo, S. Scalese, G. Impellizzeri, L. Romano, V. Privitera, J. Photochem. Photobiol. A: Chem. 321 (2016) 1–11.

[29] A. Di Mauro, M. Zimbone, M. E. Fragalà, G. Impellizzeri, Mater. Sci. Semicond. Process. 42 (2016) 98–101.

[30] M. E. Fragalà, Y. Aleeva, G. Malandrino, Thin Solid Films 22 (2011) 7694-7701.

[31] M. E. Fragalà, Y. Aleeva, G. Malandrino, Superlattices Microstruct. 48 (2010) 408.

[32] R. Wang, K. Hashimoto, A. Fujishima, M. Chikuni, E. Kojima, A. Kitamura, M.Shimohigoshi, T. Watanabe, Nature 388 (1997) 431–432.

[33]S. Chakrabarti, B. K. Dutta, J. Hazard. Mater. B112 (2004) 269-278

[34]C. I. Behnajady, N. Modirshahla, R. Hamzavi, J. Hazard. Mater. B133 (2006) 226-232

[35]A. Di Mauro, M. Cantarella, G. Nicotra, G. Pellegrino, A. Gulino, M. V. Brundo, V. Privitera, G. Impellizzeri, Sci. Reports 7:40895 (2017) 1-12

[36] Compendium of chemical terminology, in: A. D. McNaught, A. Wilkinson(Eds.), The Gold Book, 2nd edn, Blackwell Scientific Publications, Oxford, 1997.

[37] M. N. Chong, B. Jin, C.W.K. Chow, C. Saint, Water Res. 44 (2010) 2997–3027.

[38] M. Naoari, J. Malm, R. Lehto, J. Julin, K. Arstila, T. Sajavaara, M. Lahtinen, J. Vac. Sci. Technol. A 33(1) (2015) 01A128-1-7

[39] A . Di Mauro, M. Cantarella, G. Nicotra, V. Privitera, G. Impellizzeri, Appl. Catal. B: Environ. 196 (2016) 68–76.

[40] J. Tauc In Amorphous and Liquid Semiconductors: Plenum: New York, 1974, pp. 172-178.

[41] B. D. Viezbicke, S. Patel, B. E. Davis, D. P. Birnie III, Phys. Status Solidi B 8 (2015) 1700-1710.

[42] Ü. Özgür, I. Ya. Alivov, C. Liu, A. Teke, M.A. Reshchikov, S. Doan, V. Avrutin, S. J.Cho, H. Morkoc¸ J. Appl. Phys. 98 (041301) (2005) 1–303.

[43] Oxygen rich silicon thin films for photovoltaic applications, G. Di Martino, thesis, p.43, 2008, http://biblioteca.ssc.unict.it/cgi-bin/koha/opac-detail.pl?biblionumber=3189

[44] V. Scuderi, M. A. Buccheri, G. Impellizzeri, A. Di Mauro, G. Rappazzo, Kristin Bergum, Bengt G. Svensson, V. Privitera, Mater. Sci. Semicond. Process. 42 (2016) 32–35.

[45] A. Di Mauro, M. Zimbone, M. Scuderi, G. Nicotra, M. E. Fragalà, G. Impellizzeri, Nanoscale Res. Lett. 10 (2015) 484.

[46] A. G. MacDiarmid, W. E. Jones, I. D. Norris, J. Gao, A. T. Johnson, N. J. Pinto, J. Hone, B. Han, F. K. Ko, H. Okuzaki; M. Llaguno, Synth. Met. 119 (2001) 27-30.

[47] M. E. Fragalà, A. Di Mauro, D. A. Cristaldia, M. Cantarella, G. Impellizzeri, V. Privitera, J. Photochem. Photobiol. A: Chem. 332 (2017) 497–504.

[48] Y. Cao, J. Chen, H. Zhou, L. Zhu, X. Li, Z. Cao, Nanotechnology 26 (2015) 024002-024010.